International Journal of Thermophysics (2024) 45:45
https://doi.org/10.1007/s10765-024-03341-3

Thermal Conductivity Measurements for the Hydrochloroolefin R1130(E)

G. Lombardo[1,2] · D. Menegazzo[1] · M. Scattolini[1] · G. Ferrarini[1] · S. Bobbo[1] · L. Fedele[1]

Received: 30 January 2024 / Accepted: 5 February 2024 / Published online: 21 February 2024

Abstract

The identification of new refrigerants characterized by low GWP (<150), as required at international level by several agreements and regulations, is still far from the conclusion. In particular, for a proper selection, the thermophysical properties of hydro(chloro) fluoroolefins (H(C)FOs) are required, but their knowledge is still scarce for several of these fluids. Amongst these, R1130(E) has recently get some attention as a component, with R1336mzz(Z), of the azeotropic binary mixture (R514A), that could be applied as a substitute for R123 in centrifugal chillers, high-temperature heat pumps, and organic Rankine cycles. R1130(E) is a hydrochloroolefin characterized by a relatively high normal boiling temperature (320.9 K) and belongs to the ASHRAE safety group B1. Its properties are still not widely studied and, in particular, a very limited number of data is available in the peer reviewed literature for the thermal conductivity. Thus, in this paper, a set of experimental thermal conductivity data, performed with a double THW apparatus, will be presented. The data are measured in the range of temperatures between 243.15 and 313.15 K, with pressures up to 8 MPa.

Keywords R1130(E) · Thermal conductivity · Refrigerants · Low global warming potential · Thermophysical properties · Double transient hot-wire method

Selected Papers of the 22nd European Conference on Thermophysical Properties.

✉ G. Lombardo
lombardo@itc.cnr.it

[1] Construction Technologies Institute, National Research Council (CNR), Padova, Italy

[2] Department of Industrial Engineering, University of Padua (UNIPD), Padova, Italy

1 Introduction

In the current landscape of the HVAC&R industry, Hydrofluorocarbons (HFCs) have emerged as the predominant choice. However, the significant environmental impact of HFCs, particularly their high Global Warming Potential (GWP), has catalyzed a shift in focus towards more environmentally friendly, low-GWP alternatives. This shift is exemplified by major international initiatives like the Kigali Amendment to the Kyoto Protocol [1] and the F-gas Regulation on fluorinated gases (REGULATION (EU) No. 517/2014) [2]. These directives not only impose strict limitations on the use of HFCs, with a long-term GWP limit of 150 and specific application-based restrictions but also mandate a progressive reduction in the HFCs market presence, aiming for a 21% level of the baseline by 2030. The quest for new refrigerants, referred by Calm [3] as the fourth generation, involves an intricate selection process, balancing various criteria such as favorable thermodynamic properties, low toxicity, chemical stability, controlled flammability, and suitable operating pressures. A comprehensive study by Mc Linden et al. [4] significantly narrowed the field, identifying 62 possible compounds for refrigeration purposes. Among these, two categories of compound have emerged as predominant options: natural fluids (such as NH_3, CO_2 and hydrocarbons HCs) and synthetic options including hydro-fluoro-olefins (HFOs), hydro-chloro-olefins (HCFOs), and hydro-fluoro-ethers (HFEs). Notably HFOs, characterized by a carbon-carbon double bond, offer the dual advantages of a shorter atmospheric lifetime and thus lower GWP, while maintaining thermophysical properties similar to those of the HFCs they aim to replace. However, only a few applications can employ pure working fluids. In many cases, azeotropic (or near-azeotropic) blends are preferable, offering a trade-off between the characteristics of the pure fluids composing them but behaving similarly to a pure fluid. For commercial and industrial centrifugal applications, the azeotropic olefin blend R514A, consisting of cis-1,1,1,4,4-hexafluorobut-2-ene (R-1336mzz(Z)) (74.7% w.) and trans-1,2-dichloroethene (R-1130(E)) (24.3% w.), has garnered interest as a potential low-GWP and nonflammable retrofit option for R123, as well as R245fa in high-temperature industrial heat pumps, organic Rankine cycles, and centrifugal chillers [5–8]. With a 100-year GWP of just 2, R514A represents a significant environmental improvement over R123 and R245fa, whose GWPs stand at 79 and 856, respectively, as reported by the IPCC AR5 [9]. Additionally, R514A's non-flammability and classification under the ANSI/ASHRAE "B1" safety group offer practical benefits over other low-GWP refrigerants [10]. To accurately predict the properties of selected mixtures and evaluate their energy performance within thermodynamic systems, a comprehensive understanding of the thermophysical properties of each component is indispensable. This knowledge, based on reliable experimental data, plays a pivotal role in the design of efficient energy systems and the selection of suitable refrigerants for practical applications and simulations. As pointed out by Fedele et al. [11], while the properties of R1336mzz(Z) have been extensively researched [12], leading to its inclusion in the REFPROP 10.0 software [13], R1130(E) remains relatively unexplored, with no publicly available fluid equation of state despite its recent addition to ASHRAE Standard 34 [10]. A summary of the fundamental properties of R1130(E) is shown in Table 1. To date, only one thermophysical dataset is available

Table 1 Fundamental properties of the fluid used in the study. M: molar mass, T_b: boiling temperature, T_c: critical temperature, P_c: critical pressure, ρ_c: critical density, ω: acentric factor

Chemical Name	Structural formula	M [kg/kmol]	T_b [K]	T_c [K]	p_c [kPa]	ρ_c [kg/m^3]	ω
Trans-1,2-dichloroethene	ClCH=CHCl	96.94 [a]	320.9[a]	516.5[a]	5510[a]	429.93[a]	0.2137[a]

[a] Source: Tanaka et al. [14]

in the literature for trans-1,2-dicloroethene: Tanaka et al. [14] recently conducted 73 single-phase $P\rho T$ measurements of R1130(E) spanning a temperature range of 329 to 453 K and pressures up to 10.5 MPa. More recently, Lombardo et al. [15] carried out 79 experimental density measurements of compressed liquids along eight isotherms, covering a temperature range from 283.15 to 423.15 K and pressures ranging from saturation to 35 MPa. Additionally, 36 vapor pressure data points were determined using a vapor-liquid equilibrium (VLE) apparatus for temperatures between 283.15 and 353.15 K. Finally, eight saturated liquid densities were obtained by extrapolating each liquid density isotherm to its respective vapor pressure. It is important to note that, apart from the study conducted by Tanaka et al. [14], which includes 38 surface tension data points for R1130(E), measured across temperatures ranging from 228 to 373 K using the differential capillary rise method, the transport properties of trans-1,2-dichloroethene have yet to be explored. In particular, only three published data are available today on the thermal conductivity of trans-1,2-dichloroethene, measured by Bates et al. [16] at atmospheric pressure at three temperatures, i.e. 293.15, 300.15 and 313.15 K. In the context of refrigerants, thermal conductivity has particular significance for modeling processes that involve heat transfer through boiling and condensation, and its knowledge is instrumental in predicting and optimizing the performance of refrigeration systems, ensuring their efficiency and effectiveness in practical applications. To fill the substantial knowledge gap regarding the thermal conductivity of R1130(E), this study presents 48 thermal conductivity measurements under liquid conditions. These measurements span temperatures from 243.15 to 313.15 K, with pressure ranging from near saturation up to 8 MPa. The experimental data were collected using a dual Transient Hot-Wire (THW) apparatus, previously validated through testing with toluene, thus ensuring the reliability and accuracy of the obtained results.

2 Experimental

2.1 Materials

Table 2 presents details on the trans-1,2-dichloroethene (R1130(E)) sample used in this study. Sourced from Sigma-Aldrich, the sample boasts a declared purity of 99.7% by mass for the specific batch employed. Prior to conducting the experiments, the liquid sample underwent vacuum degassing to eliminate any non-condensable gases that could potentially influence the precision of the experimental results.

Table 2 Description of the R1130(E) chemical sample – purity as stated by the supplier

Chemical Name	*N*°CAS	Source	Initial Purity	Purification Method
Trans-1,2-dichloroethene	156-60-5	Sigma-Aldrich	0.997[b]	Vacuum degassing

[b] Mass fraction, GC analysis

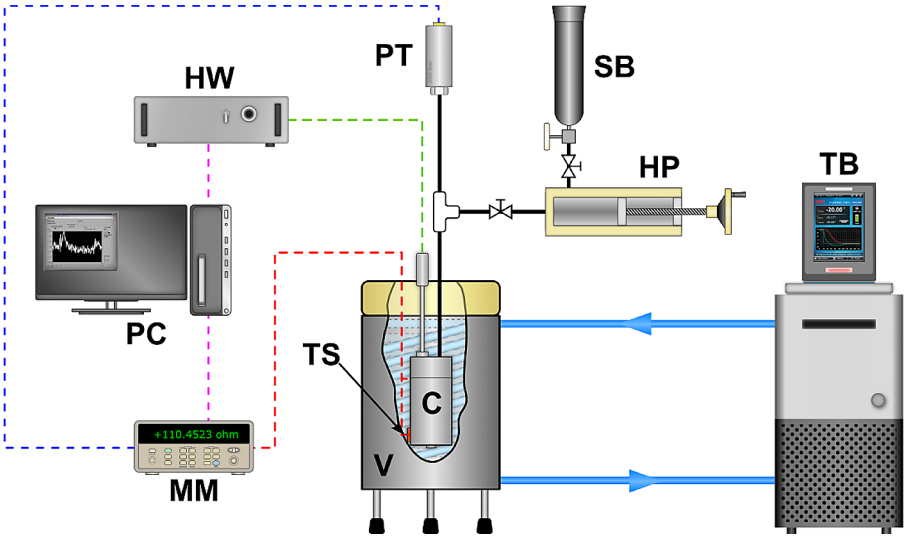

Fig. 1 Scheme of the THW apparatus, consisting of multimeter (MM), Hot Wire instrument (HW), computer (PC), pressure cell (C), thermometer (TS), pressure vessel (V), sample bottle (SB), hand-pump (HP) and thermostatic bath (TB), pressure transducer (PT).

2.2 Apparatus

The thermal conductivity measurements of R1130(E) were conducted using a TWH-01L transient hot wire instrument, manufactured by Accuinstruments. A schematic of the whole apparatus is provided in Fig. 1. This method is based on the principles outlined by Wakeham et al. [17]. The core component of the apparatus is represented by the hot wire sensor, which consists of two tantalum wires with diameters of 25 µm and lengths of 21.34 mm and 49.56 mm, respectively, the different length to compensate for end effects compared to a theoretically infinitely long wire. One wire is integrated in the two branches of a Wheatstone bridge, which provides a signal based on the resistance difference between the wires. The signal is then acquired and processed by a dedicated software, constituting the final measure. To measure the thermal conductivity of the sample, the latter was transferred from the sample bottle into a 46.6 cm^3 stainless steel pressure cell. This process involved pressurizing the sample above its saturation pressure at the highest system temperature, ensuring that the wire was fully submerged in the fluid. To maintain the desired temperature during the measurements the pressure cell was placed in a vessel filled with a secondary fluid, i.e. distilled water for temperatures above 283.15 K and ethylene alcohol (CAS No. 64-17-5) for temperatures below. The stability of the thermostatic bath was assessed to be 0.02 K.

A platinum thermal resistance, attached to the external wall of the pressure cell and connected to an Agilent 34970A multimeter, provided temperature readings with an accuracy of 0.05 K, giving an overall temperature measurement uncertainty of 0.07 K. Pressure adjustments were made using a hand pump, connected to the cell via a 1/16" stainless steel tube, as depicted in Fig. 1. The pressure was measured using a Druck PMP 4070 pressure transducer with a full scale of 13.5 MPa and an estimated uncertainty of 0.04% FS. Before conducting the experiments, the accuracy of the thermal apparatus was validated by measuring the thermal conductivity of toluene at atmospheric pressure across four temperatures ranging from 281 to 323 K. The results of these measurements, as reported by Menegazzo et al. [18], were aligned with the correlation by Assael et. al [19] implemented in REFPROP 10.0 [13] for toluene, showing deviations within ±2%, which is below the 3% uncertainty range of the model. The measurements were performed along eight isotherms. For each isotherm, the sample was compressed using the hand pump to ensure its liquid state, and pressure increased at regular intervals from close to vapor pressure up to 8 MPa. After achieving equilibrium inside the pressure cell, both in terms of pressure and temperature, the thermal conductivity was recorded. Each data point was obtained three times, with a minimum interval of 15 min between successive measurements to confirm reproducibility. The repeatability of measurements was consistently within ±0.1% scatter limits.

2.3 Uncertainty Analysis

A comprehensive analysis of uncertainty (UA) was conducted for the thermal conductivity measurements at each state point, and the corresponding findings are presented in Table 3. The overall expanded uncertainty, denoted as $U_c(\lambda)$ and calculated using Eq. (1) with a coverage factor of k=2, is summarized as follows:

$$U_c(\lambda) = k\sqrt{u_0{}^2(\lambda) + \sigma^2(\lambda) + \left[(\partial\lambda/\partial T)_p u(T)\right]^2 + \left[(\partial\lambda/\partial p)_T u(p)\right]^2} \quad k = 2 \quad (1)$$

In Eq. 1 $u_0(\lambda)$ represents the manufacturer-declared uncertainty in thermal conductivity, which is ±1%. Such uncertainty only takes into account the uncertainty related to the voltage applied to the Wheatstone bridge and the measurement of the experimental time, without considering the effects of temperature and pressure. For this purpose, the last two terms of Eq. 1 account for the influence of temperature and pressure uncertainties on the measurements, with *u(T)* and *u(p)* denoting standard uncertainties of temperature and pressure, set at 0.07 K and 0.03 bar, respectively. Given the absence of an available correlation for the thermal conductivity of R1130(E) in

Table 3 Coefficients for Eqs. (2), (3) and (4)

A_1	**A_2**	**A_3**	**A_4**	
-7.017	1.355	-1.129	-2.866	
B_1	**B_2**	**B_3**	**B_4**	
-6.117	34.996	-49.137	23.787	
C	**a**	**b**	**c**	**d**
0.128	21.363	-32.936	-86.961	193.028

the current literature, sensitivity coefficients (partial derivatives) at constant pressure and temperature, i.e., $(\partial\lambda/\partial T)_p$ and $(\partial\lambda/\partial p)_T$ were determined through linear regression of experimental data. Finally, the second term $\sigma(\lambda)$ denotes the standard deviation in thermal conductivity derived from replicated measurements of a single point, as detailed in the preceding section, and consistently falls within ±0.1% scatter limits. As a result, the uncertainties in thermal conductivity primarily stem from the uncertainty of the instrument given by the constructor, which represent the main contributor to Eq. 1. As shown in Table 3, throughout the investigated range, the final expanded uncertainty for the presented measurements remains nearly constant at 2%.

3 Results and Discussion

3.1 Measurements

A set of 48 experimental points for the thermal conductivity of R1130(E) in the liquid phase was collected. The temperature range went from 243.15 to 313.15 K, with pressures nearing saturation levels up to 8 MPa. All the experimental thermal conductivity data can be found in Table 3, and Fig. 2 visually represents the corresponding measurement conditions across temperature and pressure regions. In Fig. 2, the saturation curve was derived from data from Lombardo et al. [15], constructed using a Wagner-type correlation based on experimental data as in Eq. 2, with an average deviation AD% = 0.002% and average absolute deviation AAD% = 0.293%. Additionally, Fig. 3 illustrates the correlation between the measured thermal conductivity of liquid R1130(E) and its density, with density values sourced again from calculations by Lombardo et al. [15], performed utilizing a Tait equation based on experimental data reported in Eq. 3, with a declared average absolute deviation AAD% =

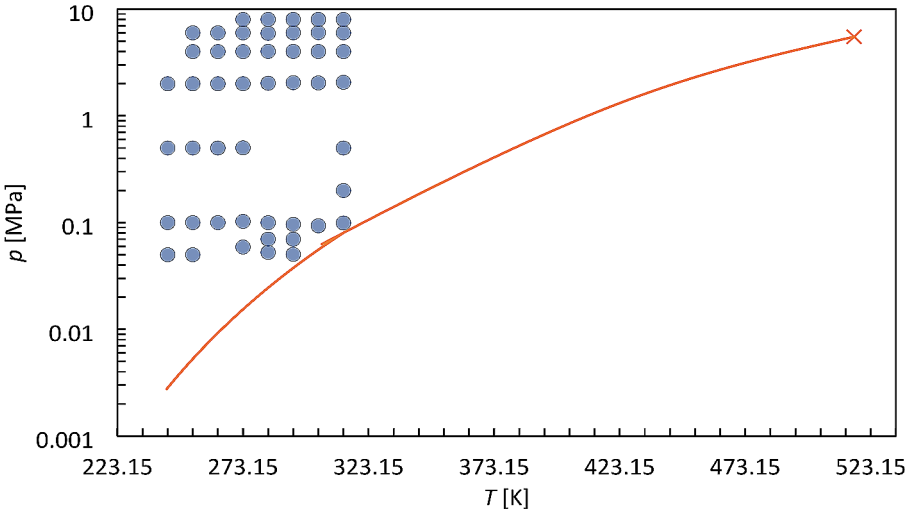

Fig. 2 Measurement points of R1130(E)

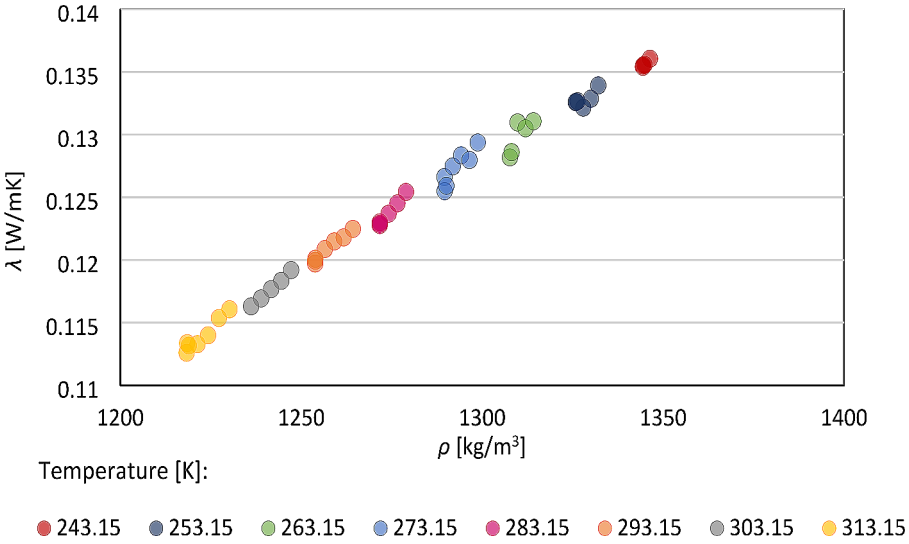

Fig. 3 Experimental thermal conductivity of R1130(E) as a function of density in the liquid region

0.052% and maximum absolute deviation MAD%=0.249%. Constants for Eqs. 2–4 are presented in Table 4.

$$T_r \ln\left(P_r\right) = A_1\tau + A_2\tau^{1.5} + A_3\tau^{2.5} + A_4\tau^5 \tag{2}$$

Here, $P_r = P_{sat}/P_c$ and $T_r = T_{sat}/T_c$ denote the reduced pressure and reduced temperature, respectively, with $\tau = 1 - \mathrm{T}/T_c$.

$$\rho^{-1} = {\rho_{sat}}^{-1}\left[1 - Cln\left(\frac{\beta + P}{\beta + P_{sat}}\right)\right] \tag{3}$$

$$\beta = P_c\left(-1 + a\tau^{1/3} + b\tau^{2/3} + c\tau + d\tau^{4/3}\right) \tag{4}$$

3.2 Data Reduction

In the context of correlating experimental data, a simplified correlation equation for the saturated liquid phase was developed based on saturation temperature. The thermal conductivity at saturation conditions was derived by extrapolating values at saturated pressure, extending measured data below 4 MPa to reach the saturated conditions. The extrapolated data were then correlated using linear fitting [20, 21], as depicted in Eq. 5:

$$\lambda_{sat,L} = -0.3183\mathrm{T}_{sat} + 212.86 \tag{5}$$

Table 4 Experimental thermal conductivity λ in R1130(E) with combined expanded uncertainty U_c[a] (k=2)

T/K	p/bar	λ /Wm^{-1}K^{-1}	U_c / Wm^{-1}K^{-1}	T/K	p/bar	λ /Wm^{-1}K^{-1}	U_c / Wm^{-1}K^{-1}
243.15	0.50	0.1354	0.0027	283.15	1.00	0.1230	0.0025
243.15	1.00	0.1355	0.0027	283.15	20.22	0.1237	0.0025
243.15	5.00	0.1356	0.0027	283.15	40.18	0.1245	0.0025
243.15	20.00	0.1361	0.0027	283.15	59.36	0.1254	0.0025
253.15	0.50	0.1326	0.0027	283.15	80.09	0.1257	0.0025
253.15	1.00	0.1326	0.0027	293.15	0.50	0.1197	0.0024
253.15	5.00	0.1327	0.0027	293.15	0.70	0.1199	0.0024
253.15	20.00	0.1322	0.0026	293.15	0.96	0.1201	0.0024
253.15	40.00	0.1329	0.0027	293.15	20.47	0.1209	0.0024
253.15	60.00	0.1339	0.0027	293.15	40.17	0.1215	0.0024
263.15	1.00	0.1282	0.0026	293.15	60.11	0.1218	0.0024
263.15	5.00	0.1286	0.0026	293.15	80.00	0.1225	0.0024
263.15	20.00	0.1310	0.0026	303.15	0.93	0.1163	0.0023
263.15	40.00	0.1305	0.0026	303.15	20.36	0.1169	0.0023
263.15	60.00	0.1311	0.0026	303.15	40.06	0.1177	0.0024
273.15	0.59	0.1266	0.0025	303.15	60.24	0.1183	0.0024
273.15	1.02	0.1255	0.0025	303.15	80.04	0.1192	0.0024
273.15	5.02	0.1259	0.0025	313.15	0.99	0.1126	0.0023
273.15	20.01	0.1275	0.0025	313.15	2.00	0.1134	0.0023
273.15	40.00	0.1283	0.0026	313.15	5.00	0.1132	0.0023
273.15	60.00	0.1280	0.0026	313.15	20.62	0.1133	0.0023
273.15	80.00	0.1294	0.0026	313.15	40.03	0.1140	0.0023
283.15	0.53	0.1229	0.0025	313.15	60.04	0.1154	0.0023
283.15	0.70	0.1228	0.0025	313.15	80.05	0.1161	0.0023

[a] Standard uncertainties u are $u(T)=0.07$ K, and $u(p)=0.03$ bar

Figure 4 illustrates the variations between extrapolated and calculated data obtained through the linear fitting of thermal conductivity with saturation temperature. The corresponding values are presented in Table 5, serving as references for the thermal conductivity of R1130(E) under saturation conditions across the temperature range from 243.15 to 313.15 K. Results demonstrate a good agreement between extrapolated and calculated data, with a MAD of 0.45% and an AAD of 0.17%.

In the investigation of thermal conductivity within the compressed liquid state, temperature and pressure have the most significant influence on this property. Figure 5a and b depict the behavior of experimentally measured thermal conductivity as a function of reduced temperature and pressure, respectively. Here, the reduced temperature ($T_r = T/T_c$, where T_c represents the critical temperature) and pressure ($P_r = P/P_c$, where P_c denotes the critical pressure) are plotted along the x-axis.

Recent years have witnessed the emergence of numerous empirical and semi-empirical models aimed at determining liquid thermal conductivity as a function of temperature and pressure, with some specifically designed for describing the thermal conductivity of liquid refrigerants.

A new dataset comprising 447 thermal conductivity data points measured along six isotherms spanning the temperature range of 240 to 340 K and pressures up to 25 MPa was provided to the authors through private communication by Al-Barghouti et al. [22]. The experimental data were employed by Al-Barghouti et al. [22] to calibrate the parameters of an ECS model, utilizing a volume-translated Peng-Robinson equation of state to furnish the necessary thermodynamic properties for model application. The ECS model represented the experimental data within its associated uncertainty of 1.4%. In Fig. 6, a comparative analysis between the ECS model, serving as the graphical baseline, and the experimental data obtained in this study is presented. It is noteworthy that, with the exception of two points, all data points fell within a range of ±2% deviation from the aforementioned model, aligning with the uncertainty of the dataset.

As depicted in Fig. 5a, the experimental measurements exhibit a pronounced dependency on temperature, while only a slight sensitivity to pressure is observed in Fig. 5b. This limited pressure influence can be attributed to the fact that, out of the 48 data points, 36 have a P_r value greater than 1, demonstrating a negligible pressure dependency.

To account for these findings, the pressure-independent model proposed by Di Nicola et al. [23] (declared AARD on a total of 41 fluids and 1372 experimental points: 4.9%) was applied to correlate the data, as expressed in Eq. 6:

$$\frac{\lambda_L}{\lambda_0} = aT_r + bP_c + c\omega + \left(\frac{1}{M}\right)^d + e\mu \tag{6}$$

In Eq. 6, P_c represents the critical pressure in bar, ω denotes the acentric factor, M is the molecular mass in kg/kmol, and μ is the dipole moment. However, given that R1130(E) possesses a zero-dipole moment [24], the last term, eμ, is omitted. The values for the remaining coefficients λ_0, a, b, c, and d are adopted from Tomassetti et al. (2020) [25], who conducted a critical review of several pressure-dependent and independent models for the thermal conductivity of liquids and re-fitted the coefficients of Eq. 6 for six low global warming potential refrigerants at reduced temperatures T_r up to 0.9 (declared AARD on a total of 6 fluids and 2073 experimental points: 1.45%, MARD: 8.48%). Fur-

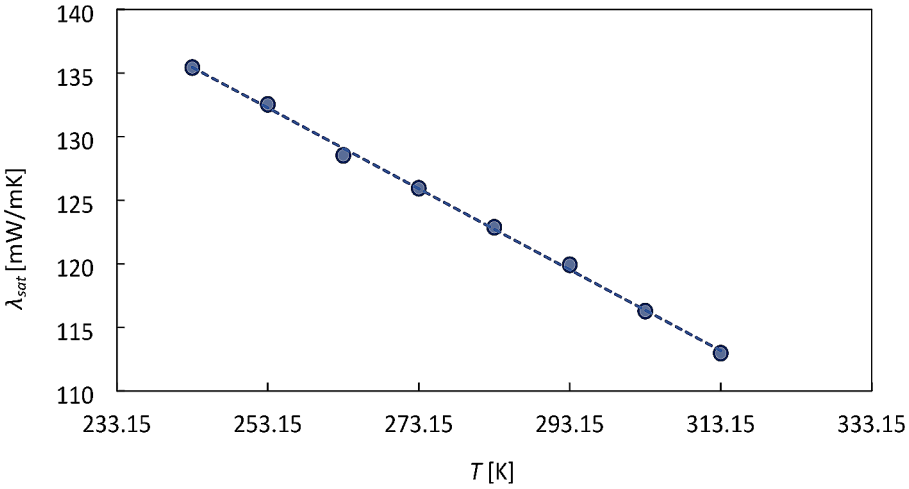

Fig. 4 Thermal conductivity in saturation condition at liquid phase. Solid points: extrapolated data; dashed line: correlated data as in Eq. 5

Table 5 Extrapolated thermal conductivity data at saturation condition and deviations from correlated data as in Eq. 5: $e = 100*(\lambda_{sat,\,extr}-\lambda_{sat,\,calc})/\,\lambda_{sat,\,extr}$

T_{sat} / K	p_{sat} / kPa	$\lambda_{sat,L\,ext}$ / W·m^{-1}K^{-1}	e
243.15	2.84	0.1354	-0.03%
253.15	5.28	0.1325	0.19%
263.15	9.25	0.1285	-0.45%
273.15	15.40	0.1259	0.02%
283.15	24.52	0.1229	0.11%
293.15	37.57	0.1199	0.31%
303.15	55.69	0.1163	-0.08%
313.15	80.17	0.1130	-0.19%

thermore, in their study, Tomassetti et al. [25] developed the pressure-dependent model presented in Eq. 7, based on the model by Di Nicola et al. [23] from Eq. 6, which accounts for the liquid thermal conductivity's dependence on temperature while considering the effect of pressure, typically relevant for P_r values greater than 1:

$$\frac{\lambda_L(P_r)}{\lambda_0} = \left[aT_r + bP_c + c\omega + \left(\frac{1}{M}\right)^d\right]\left[1 + (f_0 + fT_r^2)P_r^g\right] \tag{7}$$

The values of λ_0, a, b, c, d remain consistent with those reported in Table 6 for Eq. 6, with the addition of the regressed values for f_0, f, and g.

Figure 7 illustrates the deviations between the experimentally measured thermal conductivity (λ) data, from this work and from the communicated dataset from NIST, and the values calculated using both the pressure-independent model by Di Nicola et al. [23], with the re-fitted coefficients by Tomassetti et al. [25]. In Fig. 7 deviations are represented as function of reduce temperature T_r, (a) and reduced pressure, P_r, (b), the baseline representing the model in Eq. 6. On the other hand, Fig. 8a and b displays deviations between

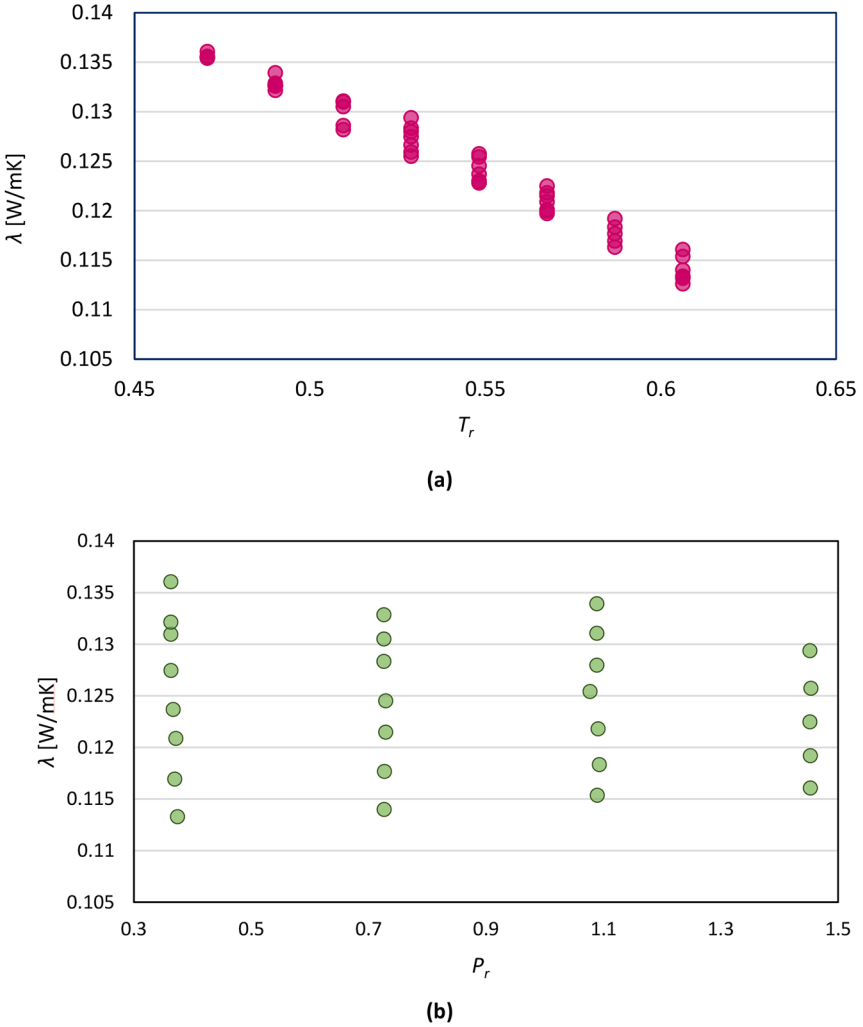

Fig. 5 Experimental liquid thermal conductivity λ data for R1130(E) as function of reduced temperature, T_r, (a) and reduced pressure, P_r, (b)

the available data sets for thermal conductivity of R1130(E) and the pressure-dependent model of Eq. 7. as function of T_r and P_r, respectively.

When looking at the CNR dataset from this work Eq. 6 and Eq. 7 exhibit similar behaviour, both overestimating the data with deviations up to 6.71% for Eqs. 6 and 6.91% for Eq. 7, and AARD of 3.11% and 3.87%, respectively. This suggesting that the models perform comparably when predicting thermal conductivity for the CNR experimental conditions. Examining trends as a function of reduced temperature (Figs. 7a and 8a) and reduced pressure (Figs. 7b and 8b), the deviations for both models closely align, indicating similar predictive accuracies for this set of experimental data and no significant difference in how each model handles temperature and pressure variations in this dataset.

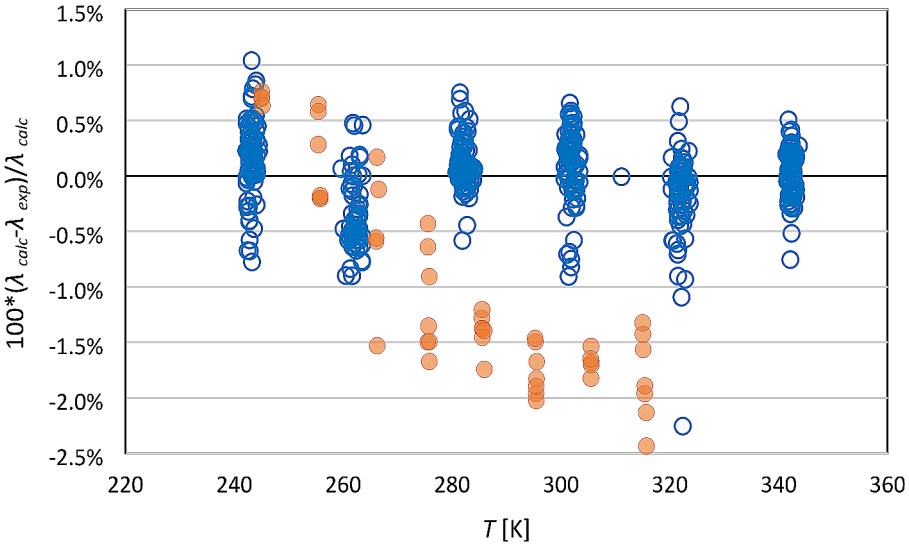

Fig. 6 Deviations between the ECS model from Al-Barghouti et al. [22] and experimental data as function of temperature. Solid points: experimental data from this work; empty points: experimental data from Al-Barghouti et al. [22]

Table 6 Coefficients of Eq. 6 and Eq. 7 from Tomassetti et al. (2020) [25]

λ_0	a	b	c	d	f_0	f	g
0.43693	-0.28725	0.00372	0.26967	0.36436	-0.00135	0.05484	0.88049

shifting the focus to the dataset from Al-Barghouti et al. [22], which covers a wider range of pressures and temperatures, more pronounced differences emerge between the two models. The pressure-independent model from Eq. 6 generally exhibits smaller deviations (MARD=10.02%, AARD=3.10%, compared to MARD=5.10%, AARD=11.10% for the pressure-dependent model in Eq. 7), indicating a closer fit to the experimental data; however, this model demonstrates greater variability in deviations with pressure changes (Fig. 7b), suggesting that this model may be more sensitive to pressure variations or less accurate under certain pressure conditions. Overall, despite greater variability in results, the pressure-dependent model as in Eq. 6 holds a slight edge in predictive accuracy for both experimental datasets. Finally, when considering the pressure-dependent model, the results for the experimental data measured in this work align with the findings reported by Tomassetti et al. [20] for the other six low GWP refrigerants considered in their study. However, significantly higher deviations are observed for the communicated dataset from Al-Barghouti et al. [22], indicating that the accuracy of the models, as declared by Tomassetti et al. [20], no longer holds true for R1130(E) under larger temperature and pressure ranges.

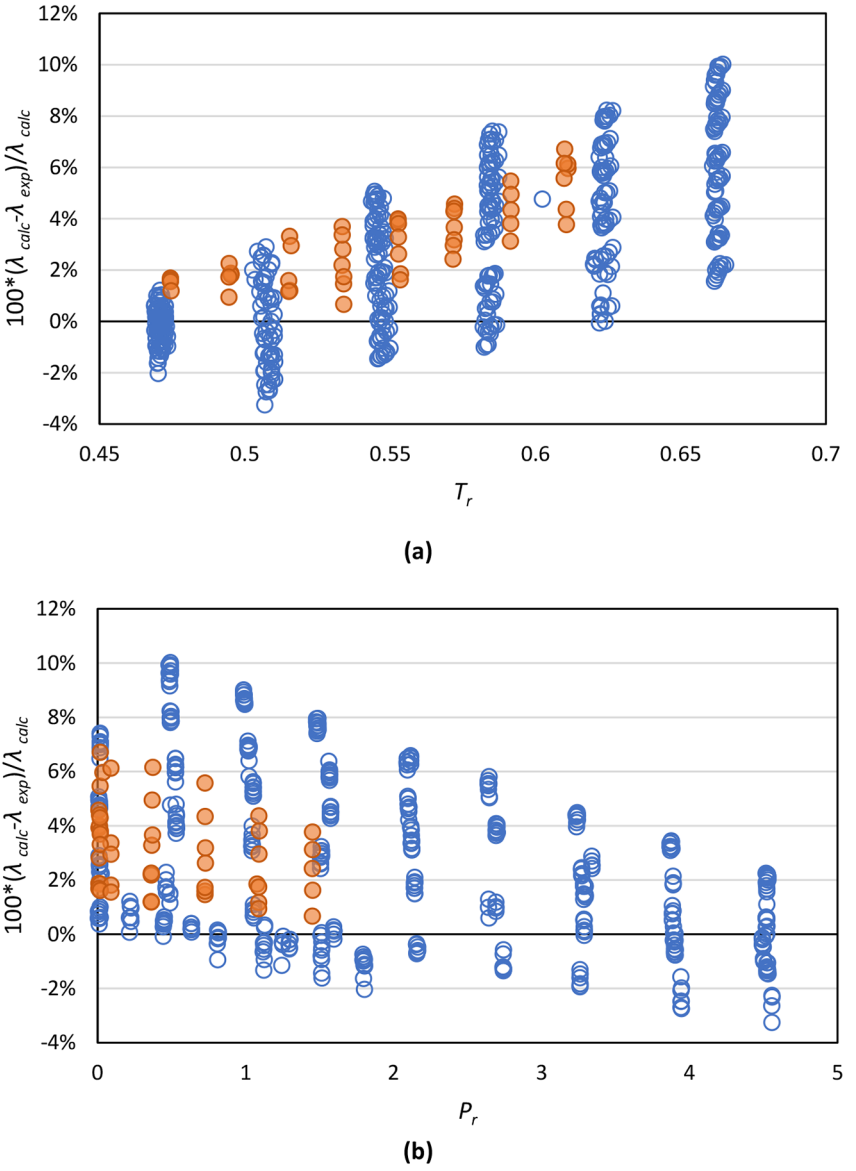

Fig. 7 Deviations between Eq. 6 and experimental data as function of reduced temperature, T_r, (a) and reduced pressure, P_r, (b). Solid points: experimental data from this work; empty points: experimental data from Al-Barghouti et al. [22]

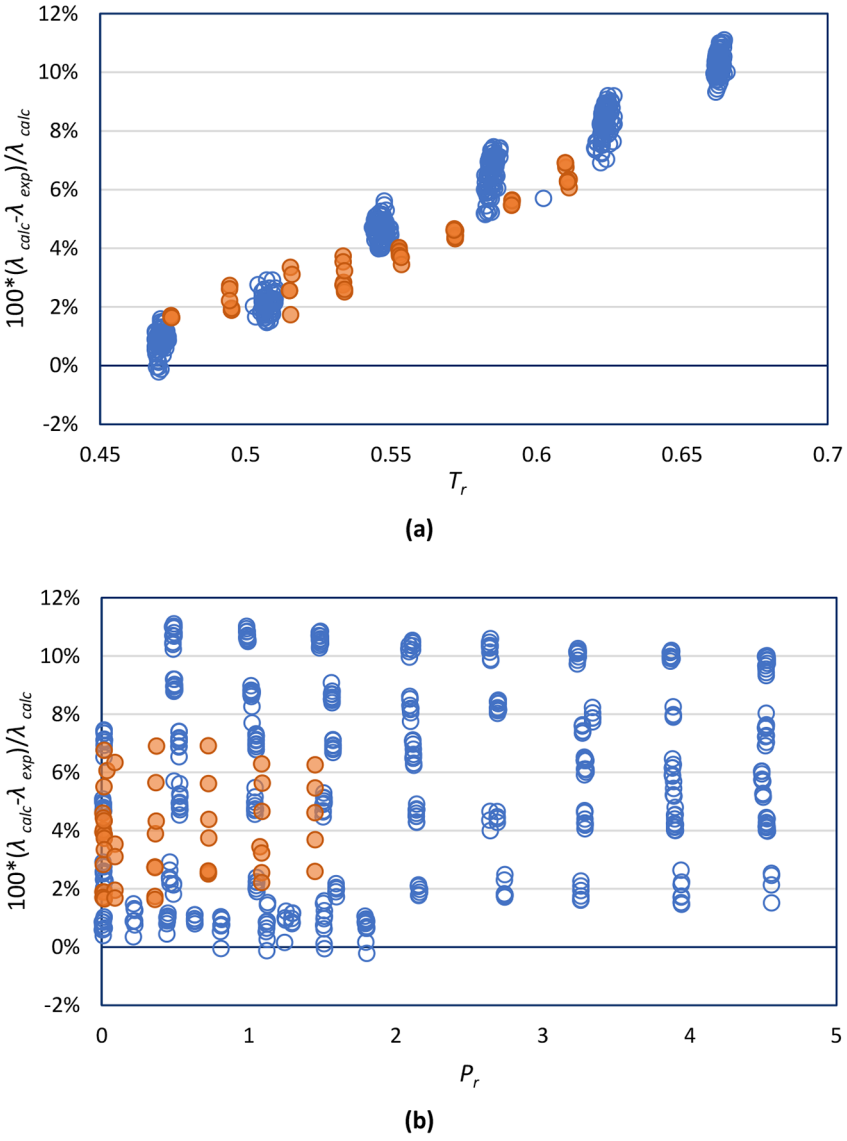

Fig. 8 Deviations between Eq. 7 and experimental data as function of reduced temperature, T_r, (a) and reduced pressure, P_r, (b). Solid points: experimental data from this work; empty points: experimental data from Al-Barghouti et al. [22]

4 Conclusions

The quest for environmentally friendly refrigerants has recently turned towards trans-1,2-dichloroethene, referred to as R1130(E), as a constituent in the olefin azeotropic binary mixture R514A. This mixture has application suitability in industrial high-temperature heat pumps, Organic Rankine Cycles (ORC), and centrifugal chillers. Despite

the growing interest in R1130(E) as a refrigerant, no thermal conductivity dataset exists in the current literature. Hence, this study addresses this gap by employing the transient hot-wire technique to measure the thermal conductivity of R1130(E) in its liquid phase. A total of 48 experimental data points were collected in the temperature range from 243.15 to 313.15 K, covering pressures up to 8.0 MPa. The uncertainty in thermal conductivity measurements was estimated at 2%, providing confidence in the accuracy of the acquired data. Results demonstrated a strong dependence of thermal conductivity on temperature, with less significant pressure influence. A simplified correlation for predicting thermal conductivity at the saturation state was developed using the extrapolation method and verified against experimental data, showing good agreement (MAD=0.45%; AAD=0.17%).

The pressure-independent model proposed by Di Nicola et al. [23] and the pressure-dependent model by Tomassetti et al. [25] were applied to thermal conductivity in liquid conditions and found to be quite effective for correlating the data (MAD=6.71% AAD=3.11% and MARD=6.91%; AARD=3.87%, respectively). Extending the analysis to a larger range of pressures and temperatures the pressure-independent model showcased smaller deviations for both datasets but greater variability with pressure changes, indicating sensitivity under specific conditions. Results aligned with findings by Tomassetti et al. [25] for other low GWP refrigerants, yet significant deviations were noted under broader temperature and pressure ranges. This underscores the necessity for careful model selection based on refrigerant characteristics and experimental conditions. Overall, this study provides a significant contribution to the understanding of the thermal conductivity of trans-1,2-dichloroethene, offering a valuable reference for future studies and industrial applications.

Author Contributions G.L., D.M and M.S. conducted the experiments. G.L. and D.M. analyzed the data. G.L. wrote the main manuscript text. All authors reviewed the manuscript.

Funding The authors received no financial support for the research, authorship, and/or publication of this article.

Data Availability No datasets were generated or analysed during the current study.

Declarations

Competing Interests The authors declare no competing interests.

References

1. *The Kigali Amendment to the Montreal Protocol: HFC Phase-Down* (United Nations Environment Programme, 2016)
2. European Parliament and Council of the European Union, *Regulation (EU) No 517/2014 of the European Parliament and of the Council of 16 April 2014 on Fluorinated Greenhouse Gases and Repealing Regulation (EC) No 842/2006 Text with EEA Relevance* (n.d.)
3. J.M. Calm, Int. J. Refrig. **31**, 1123 (2008)
4. M.O. McLinden, A.F. Kazakov, J.S. Brown, P.A. Domanski, Int. J. Refrig. **38**, 80 (2014)
5. P. Giménez-Prades, J. Navarro-Esbrí, C. Arpagaus, A. Fernández-Moreno, A. Mota-Babiloni, Renew. Sustain. Energy Rev. **167**, 112549 (2022)
6. K. Schultz, E. Gallan, in *ASHRAE Winter Conf* (2017)

7. G. Li, J. Eng. Thermophys. **31**, 340 (2022)
8. R.A. Yıldırım, A. Özhan, K. Kazım, Journal. **5**, 45 (2022)
9. IPCC, *Climate Change 2013 – The Physical Science Basis* (Cambridge University Press, Cambridge, United Kingdom and New York, NY, USA, 2014)
10. *ANSI/ASHRAE Standard 34-2019, Designation and Safety Classification of Refrigerants* (2019)
11. L. Fedele, G. Lombardo, I. Greselin, D. Menegazzo, S. Bobbo, Int. J. Thermophys. **44**, 80 (2023)
12. M.O. McLinden, R. Akasaka, J. Chem. Eng. Data. **65**, 4201 (2020)
13. E.W. Lemmon, I.H. Bell, M.L. Huber, M.O. McLinden, *NIST Standard Reference Database 23: Reference Fluid Thermodynamic and Transport Properties-REFPROP, Version 10.0, National Institute of Standards and Technology* (2018)
14. K. Tanaka, C. Kondou, S. Fukuda, R. Akasaka, Int. J. Thermophys. **43**, 69 (2022)
15. G. Lombardo, D. Menegazzo, L. Fedele, S. Bobbo, M. Scattolini, in *Refrig. Sci. Technol. PROCEEDINGS, 26th IIR Int. Congr. Refrig*, edited by Association Française du Froid (AFF) (International Institute of Refrigeration (IIR), Paris, 2023), pp. 113–122
16. O.K. Bates, G. Hazzard, G. Palmer, Ind. Eng. Chem. **33**, 375 (1941)
17. W.A. Wakeham, A. Nagashima, J.V. Sengers, I. U. Of pure, and A. C. C. on Thermodynamics, *Measurement of the Transport Properties of Fluids* (Blackwell Scientific, 1991)
18. D. Menegazzo, G. Lombardo, M. Scattolini, G. Ferrarini, S. Rossi, L. Fedele, S. Bobbo, Thermal Conductivity Measurements for trans-1,3,3,3-Tetrafluoropropene (R1234ze(E)) in Liquid Phase, Int. J. Refrig. (2023) (submitted)
19. M.J. Assael, S.K. Mylona, M.L. Huber, R.A. Perkins, J. Phys. Chem. Ref. Data. **41**, 023101 (2012)
20. M.J. Alam, M.A. Islam, K. Kariya, A. Miyara, Int. J. Refrig. **90**, 174 (2018)
21. D. Mondal, K. Kariya, A.R. Tuhin, K. Miyoshi, A. Miyara, Int. J. Refrig. **129**, 109 (2021)
22. K.S. Al-Barghouti, A.J. Rowane, I.H. Bell, M.L. Huber, R.A. Perkins, Thermal conductivity of Liquid trans-1,2-Dichloroethene (R-1130(E)): measurement and modeling. Int. J. Thermophys. (2024) (accepted).
23. G. Di Nicola, E. Ciarrocchi, G. Coccia, M. Pierantozzi, Int. J. Refrig. **45**, 168 (2014)
24. V.A. Mikhailov, M.A. Parkes, R.P. Tuckett, C.A. Mayhew, J. Phys. Chem. A **110**, 5760 (2006)
25. S. Tomassetti, G. Coccia, M. Pierantozzi, G. Di Nicola, Int. J. Refrig. **117**, 358 (2020)